J|A|C|S
ARTICLES
Published on Web 08/13/2002

Multifrequency EPR Study and Density Functional g-Tensor Calculations of Persistent Organorhenium Radical Complexes

Stéphanie Frantz,[†] Heiko Hartmann,[†] Natasa Doslik,[†] Matthias Wanner,[†] Wolfgang Kaim,*[,†] Hans-Jürgen Kümmerer,[‡] Gert Denninger,[‡] Anne-Laure Barra,[§] Carole Duboc-Toia,[§] Jan Fiedler,[||] Ilaria Ciofini,[⊥] Christian Urban,[⊥] and Martin Kaupp*[,⊥]

Contribution from the Institut für Anorganische Chemie, Universität Stuttgart, Pfaffenwaldring 55, D-70550 Stuttgart, Germany, 2. Physikalisches Institut, Universität Stuttgart, Pfaffenwaldring 57, D-70550 Stuttgart, Germany, Laboratoire des Champs Magnétiques Intenses, CNRS, F-38042 Grenoble, France, J. Heyrovsky Institute of Physical Chemistry, Academy of Sciences of the Czech Republic, Dolejškova 3, CZ-18223 Prague, Czech Republic, and Institut für Anorganische Chemie, Universität Würzburg, Am Hubland, D-97074 Würzburg, Germany

Received February 6, 2002

Abstract: The dinuclear radical anion complexes $\{(\mu\text{-L})[Re(CO)_3Cl]_2\}^{\bullet-}$, L = 2,2′-azobispyridine (abpy) and 2,2′-azobis(5-chloropyrimidine) (abcp), were investigated by EPR at 9.5, 94, 230, and 285 GHz (abpy complex) and at 9.5 and 285 GHz (abcp complex). Whereas the X-band measurements yielded only the isotropic metal hyperfine coupling of the ^{185,187}Re isotopes, the high-frequency EPR experiments in glassy frozen CH_2Cl_2/toluene solution revealed the *g* components. Both the $a(^{185,187}Re)$ value and the *g* anisotropy, $g_1 - g_3$, are larger for the abcp complex, which contains the better π-accepting bridging ligand. Confirmation for this comes also from IR and UV/vis spectroscopy of the new $\{(\mu\text{-abcp})[Re(CO)_3Cl]_2\}^{o/\bullet-/2-}$ redox system. The *g* values are reproduced reasonably well by density functional calculations which confirm higher metal participation at the singly occupied MO and therefore larger contributions from the metal atoms to the *g* anisotropy in abcp systems compared to abpy complexes. Additional calculations for a series of systems $\{(\mu\text{-abcp})[M(CO)_3X]_2\}^{\bullet-}$ (M = Tc or Re and X = Cl, and X = F, Cl, or Br with M = Re) provided further insight into the relationship between spin density distribution and *g* anisotropy.

Complexes of tricarbonylchlororhenium, $Re(CO)_3Cl$, with α-diimine radical anions such as $bpy^{\bullet-}$ (bpy = 2,2′-bipyridine) have become interesting as the primary activated intermediates in photo- or electrocatalytic cycles of CO_2 reduction.[1,2]

$$(bpy)Re(CO)_3Cl + e^- \rightarrow [(bpy)Re(CO)_3Cl]^{\bullet-} \xrightarrow[+CO_2]{-Cl^-} [(bpy)Re(CO)_3(CO_2)]^{\bullet-} \rightarrow \rightarrow$$

Although $[(bpy)Re(CO)_3Cl]^{\bullet-}$ and related "Re(0)" species have been characterized as rhenium(I) containing radical complexes by X-band EPR in fluid solution,[3−5] their full EPR analysis was precluded by the dominant ^{185,187}Re hyperfine splitting (for ^{185}Re, 37.4% natural abundance, $I = 5/2$, isotropic hyperfine constant $a_o = 1253.60$ mT; for ^{187}Re, 62.6%, $I = 5/2$, $a_o = 1266.38$ mT).[6] This splitting and the broadness of the individual lines due to quadrupolar effects and unresolved ^{35,37}Cl hyperfine coupling ($I = 3/2$) not only obscured ^{1}H and ^{14}N hyperfine information from the spin-bearing ligand[3−5] but also prevented resolution of the *g* components in frozen solution at X-band frequency (9.5 GHz).

Herein we report a multifrequency EPR investigation of two stable dinuclear complex anions $\{(\mu\text{-L})[Re(CO)_3Cl]_2\}^{\bullet-}$, L = 2,2′-azobispyridine (abpy,[3,7] complex **1**) and 2,2′-azobis(5-chloropyrimidine) (abcp, complex **2**).[7,8]

These compounds are highly suitable for a detailed experimental and computational study for the following reasons:

(i) Both paramagnetic species are persistent under ambient conditions, so in situ generation methods did not have to be applied. This advantage was crucial for the 230 and 285 GHz measurements, where the wavelengths are 1.30 and 1.05 mm, respectively.

* Authors to whom correspondence should be addressed. E-mail: kaim@iac.uni-stuttgart.de (W.K.).
[†] Institut für Anorganische Chemie, Universität Stuttgart.
[‡] Physikalisches Institut, Universität Stuttgart.
[§] Laboratoire des Champs Magnétiques Intenses, Grenoble.
[||] J. Heyrovsky Institute of Physical Chemistry, Prague.
[⊥] Institut für Anorganische Chemie, Universität Würzburg.

(1) (a) Sullivan, B. P.; Meyer, T. J. *J. Chem. Soc., Chem. Commun.* **1984**, 1244. (b) Hawecker, J.; Lehn, J. M.; Ziessel, R. *Helv. Chim. Acta* **1986**, *69*, 1900. (c) Ziessel, R. In *Photosensitization and Photocatalysis Using Inorganic and Organometallic Compounds*; Kalyanasundaram, K., Grätzel, M., Eds.; Kluwer: Dordrecht, 1993; p 217.
(2) (a) Johnson, F. P. A.; George, M. W.; Hartl, F.; Turner, J. J. *Organometallics* **1996**, *15*, 3374. (b) Scheiring, T.; Klein, A.; Kaim, W. *J. Chem. Soc., Perkin Trans. 2* **1997**, 2569.
(3) Kaim, W.; Kohlmann, S. *Chem. Phys. Lett.* **1987**, *139*, 365.
(4) Kaim, W.; Kohlmann, S. *Inorg. Chem.* **1990**, *29*, 2909.
(5) Klein, A.; Vogler, C.; Kaim, W. *Organometallics* **1996**, *15*, 236.
(6) Weil, J. A.; Bolton, J. R.; Wertz, J. E. *Electron Paramagnetic Resonance*; Wiley: New York, 1994; p 536.
(7) Kaim, W. *Coord. Chem. Rev.* **2001**, *219−221*, 463.
(8) Doslik, N.; Sixt, T.; Kaim, W. *Angew. Chem.* **1998**, *110*, 2521; *Angew. Chem., Int. Ed.* **1998**, *37*, 2403.

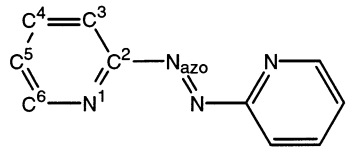

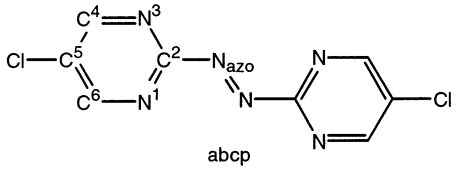

formula 1

(ii) The known abpy complex[3,9] and the new abcp compound exhibit very strong metal/ligand interaction because these azo ligands[7] have very low-lying π^* orbitals, with the main contribution coming from the four coordinating nitrogen centers.[10] Accordingly, a relatively large ^{185,187}Re hyperfine coupling of 2.54 mT has already been reported for $\{(\mu\text{-abpy})[\text{Re}(\text{CO})_3\text{Cl}]_2\}^{\bullet-}$.[3,4] Anion radicals $(\text{NR})_2^{\bullet-}$ of azo compounds are formally related via NR≙O to the superoxide ion $O_2^{\bullet-}$, which can also act as a bridging radical ligand in dinuclear complexes.

(iii) The abcp ligand has been established as an even better π acceptor than abpy by example of a structurally characterized dicopper(I) compound.[8]

(iv) The structure of neutral $(\mu\text{-abpy})[\text{Re}(\text{CO})_3\text{Cl}]_2$ in the anti (trans) configuration has been reported recently,[9] serving as a starting point for structure optimization by quantum chemical methods.

(v) The present dinuclear complexes are challenging from a fundamental EPR theory point of view: Qualitative models for the interpretation and prediction of electronic **g**-tensors have long been available both for simple organic π radicals[11] and for "normal" transition metal complexes with largely metal-centered spin density.[12] These types of models are lacking for complexes in which the spin density is largely but not entirely centered on the ligand. Here we hope to be able to develop improved qualitative concepts based on the results of quantitative quantum chemical calculations.

The calculations were performed both for the experimentally characterized ligands and complexes and for the as-yet unknown complexes of $\text{abcp}^{\bullet-}$ with $\text{Tc}(\text{CO})_3\text{Cl}$ and $\text{Re}(\text{CO})_3\text{X}$ (X = F, Br), to gain deeper insight into the influence of both the metal atoms and the halogens on the anisotropy and orientation of the **g**-tensor.

Experimental Section

Instrumentation. X-band EPR spectra were recorded on a Bruker System ESP 300 equipped with a Bruker ER035M gaussmeter and a HP 5350B microwave counter. The W-band spectrum (94 GHz) was

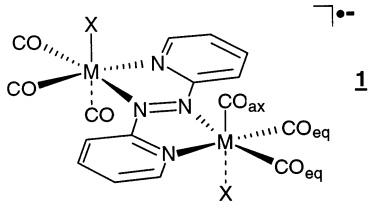

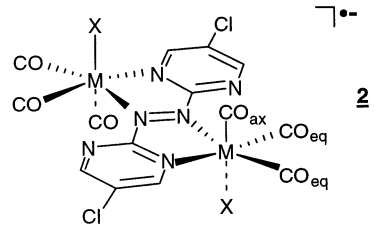

formula 2

obtained using a Bruker ELEX SYS E680 spectrometer; due to the small sample size, the signal-to-noise ratio was less favorable in this experiment. High-frequency EPR spectroscopy above 200 GHz was performed using a multifrequency spectrometer.[13] Gunn diodes operating at 95 and 115 GHz and equipped with a second and third harmonic generator have been used as a radiation source. An InSb bolometer (QMC Instruments) was used for detection. The main magnetic field was provided by a superconducting magnet (Cryogenics Consultant) which generates fields up to 12 T. Owing to different field sweep conditions, the absolute values of the *g* components were obtained by calibrating the precisely measured *g* anisotropy data with the isotropic *g* value from X-band measurements. While this procedure does not account for the temperature dependence of *g*, the values extracted are identical with those obtained using an added standard. ^{1}H NMR spectra were taken on a Bruker AC 250 spectrometer, and infrared spectra were obtained using a Perkin-Elmer Paragon 1000 FTIR instrument. UV/vis/NIR absorption spectra were recorded on a Bruins Instruments Omega 10 spectrophotometer. Cyclic voltammetry was carried out at 100 mV/s scan rate in dichloromethane/0.1 M Bu_4NPF_6 using a three-electrode configuration (glassy carbon working electrode, Pt counter electrode, Ag/AgCl reference) and a PAR 273 potentiostat and function generator. The ferrocene/ferrocenium couple served as internal reference. IR and UV/vis/NIR spectroelectrochemical measurements were performed using an optically transparent thin-layer electrode (OTTLE) cell.[14] A two-electrode capillary[15] was used for EPR spectroelectrochemistry in the X-band.

$\{(\mu\text{-abcp})[\text{Re}(\text{CO})_3\text{Cl}]_2\}$. An amount of 145 mg (0.40 mmol) of $\text{Re}(\text{CO})_5\text{Cl}$ in 10 mL of CH_2Cl_2 was treated with 51 mg (0.20 mmol) of abcp[8] and 25 mL of chlorobenzene. Controlled heating for 2 h at 75 °C produced a green solution. Removal of the solvents, re-solvation in dichloromethane, precipitation with diethyl ether, and recrystallization from CH_2Cl_2 gave the green complex in 137 mg (79%) yield. Anal. Calcd for $\text{C}_{14}\text{H}_4\text{Cl}_4\text{N}_6\text{O}_6\text{Re}_2$ (866.36): C, 19.41; H, 0.47; N, 9.70. Found: C, 19.77; H, 0.50; N, 9.57. ^{1}H NMR (CD_2Cl_2): δ = 9.23 (d, $\text{H}^{6,6'}$), 8.94 (d, $\text{H}^{4,4'}$) ppm; J = 2.6 Hz. IR (CH_2Cl_2): ν_{CO} = 2017, 1956 (br) cm^{-1}. UV/vis/NIR (CH_2Cl_2): λ_{max} (ϵ) = 903 (9220), 815sh, 356 (12 760), 324 (12 540) nm (M^{-1} cm^{-1}). $E_{1/2}$(red1) = 0.09 V, $E_{1/2}$(red2) = −0.64 V vs $[\text{Fe}(\text{C}_5\text{H}_5)_2]^{+/0}$ in CH_2Cl_2/0.1 M Bu_4NPF_6. Under refluxing conditions or after prolonged storage, the green solution turned purplish red, to yield a paramagnetic product containing $\{(\mu\text{-abcp})[\text{Re}(\text{CO})_3\text{Cl}]_2\}^{\bullet-}$ (**2**), which could also be obtained spectroelectrochemically from the neutral complex. IR (CH_2Cl_2): ν_{CO} = 2010, 1925,

(9) Hartmann, H.; Scheiring, T.; Fiedler, J.; Kaim, W. *J. Organomet. Chem.* **2000**, *604*, 267.
(10) Kaim, W.; Kohlmann, S. *Inorg. Chem.* **1986**, *25*, 3306. (b) Kaim, W.; Kohlmann, S. *Inorg. Chem.* **1987**, *26*, 68.
(11) See: (a) Stone, A. J. *Proc. R. Soc. A* **1963**, *271*, 424. (b) Stone, A. J. *Mol. Phys.* **1964**, *6*, 316.
(12) See, e.g.: (a) Abragam, A.; Pryce, M. H. L. *Proc. R. Soc. A* **1951**, *205*, 135. (b) Abragam, A.; Bleaney, B. *Electron Paramagnetic Resonance of Transition Ions*; Clarendon Press: Oxford, 1970. (c) McGarvey, B. R. In *Transition Metal Chemistry: A Series of Advances, Vol. 3.*; Carlin, R. L., Ed.; New York, 1966; pp 89−201. (d) Mabbs, F. E.; Collison, D. *Electron Paramagnetic Resonance of d Transition Metal Compounds*; Elsevier: Amsterdam, 1992.
(13) Barra, A.-L.; Brunel, L.-C.; Robert, J.-B. *Chem. Phys. Lett.* **1990**, *165*, 107.
(14) Krejcik, M.; Danek, M.; Hartl, F. *J. Electroanal. Chem. Interfacial Electrochem.* **1991**, *317*, 179.
(15) Kaim, W.; Ernst, S.; Kasack, V. *J. Am. Chem. Soc.* **1990**, *112*, 173.

1898 cm^{-1}. UV/vis/NIR (CH_2Cl_2): λ_{max} (ϵ) = 761 (3000), 526 (4450), 468 (3750), 393 (14 870) nm (M^{-1} cm^{-1}).

Details of the Calculations. Details on our approach for the calculation of **g**-tensors, based on density functional theory (DFT), have been reported.[16] Herein we describe only those features necessary for the understanding of the results. The **g**-tensor is calculated as a correction to the free electron value (given in ppm), i.e.,

$$\mathbf{g} = g_e\mathbf{1} + \Delta\mathbf{g} \tag{1}$$

with $g_e = 2.002319$. Up to the level of second-order perturbation theory, the **g**-shift ($\Delta\mathbf{g}$) consists of the relevant Breit−Pauli terms,

$$\Delta\mathbf{g} = \Delta\mathbf{g}_{SO/OZ} + \Delta\mathbf{g}_{RMC} + \Delta\mathbf{g}_{GC} \tag{2}$$

The first term, which couples the perturbation due to the field-independent spin−orbit (SO) operators with the orbital Zeeman interaction (OZ), is dominant (except for extremely small $\Delta\mathbf{g}$ values). In the uncoupled density functional (UDFT) approach,[17] it is evaluated using the following expression (given in atomic units):

$$\Delta\mathbf{g}_{SO/OZ,u,v} = \frac{\alpha^2}{2} g_e \left\lfloor \sum_k^{occ(\alpha)} \sum_a^{virt(\alpha)} \frac{\langle\psi_k^\alpha|H_{SO,v}|\psi_a^\alpha\rangle \langle\psi_a^\alpha|l_{O,u}|\psi_k^\alpha\rangle}{\epsilon_k^\alpha - \epsilon_a^\alpha} - \sum_k^{occ(\beta)} \sum_a^{virt(\beta)} \frac{\langle\psi_k^\beta|H_{SO,v}|\psi_a^\beta\rangle \langle\psi_a^\beta|l_{O,u}|\psi_k^\beta\rangle}{\epsilon_k^\beta - \epsilon_a^\beta} \right\rfloor \tag{3}$$

where α is the fine structure constant, H_{SO} is the field-independent spin−orbit operator, $l_{O,u}$ is a spatial component of the orbital Zeeman operator, and u and v are Cartesian components. The ψ_i and ϵ_i are the Kohn−Sham orbitals and eigenvalues of a spin-polarized DFT calculation. At the Breit−Pauli level, the spatial part of the SO operator, H_{SO}, can be written (in atomic units) as

$$H_{SO,iu} = \frac{\alpha^2}{4} g_e \left(\sum_N \frac{Z_N L_{iNu}}{r_{iN}^3} - \sum_{j\neq i} \frac{L_{ju}^i}{r_{ij}^3} - 2\sum_{j\neq i} \frac{L_{iu}^j}{r_{ij}^3} \right) \tag{4}$$

where Z_N is the charge of nucleus N, $L_{iNu} = -i(r_{iN} \times \Delta_i)_u$, $L_{ju}{}^i = -i(r_{ij} \times \Delta_j)_u$ (r_{iN} and r_{ij} are relative electron−nucleus and electron−electron position vectors, respectively). Physically, the first term is the one-electron SO operator due to the charge of the nuclei, the second is the two-electron SO operator, and the last is the so-called spin−other−orbit term arising from the relativistic Breit interaction between the electrons.

In our treatment, the spin−orbit orbital Zeeman cross term ($\Delta\mathbf{g}_{SO/OZ}$), the relativistic mass correction ($\Delta\mathbf{g}_{RMC}$), and the one-electron contributions to the gauge corrections ($\Delta\mathbf{g}_{GC(1e)}$) are taken into account.

An accurate treatment of spin−orbit coupling is mandatory for reliable **g**-tensor calculations. A combination of all-electron and pseudopotential (effective core potential, ECP) treatment for H_{SO} has been used, based on a superposition of effectively atomic SO operators. While SO ECPs[18] have been employed for the metal atoms, as well as for Cl and Br, the all-electron atomic mean field (AMFI) SO approximation[19] was employed for all other atoms (using the AMFI program[20]). The mixed use of AMFI and SO ECP operators in the same calculation has been validated in detail previously.[16] The effectively atomic nature of the SO operators allows both the breaking-down of $\Delta\mathbf{g}_{SO/OZ}$ into atomic contributions and computations on relatively large systems, thus providing an interesting tool for the analysis of the overall **g**-tensor in transition metal complexes.

Previous DFT studies of **g**-tensors for transition metal complexes have indicated that the use of gradient-corrected (GGA) or local (LDA) density functionals underestimates the **g**-shift values significantly.[16,21] It is possible to partly correct these deficiencies by admixture of Hartree−Fock exchange in hybrid functionals.[22] In contrast, for organic radicals, GGA or LDA functionals tend to slightly *overestimate* the **g**-shifts,[16] and hybrid functionals do not appear to change this situation.[22] No experience whatsoever is available for DFT calculations of **g**-tensors on systems such as the present ligand-centered radical complexes. All calculations in this work were performed at the gradient-corrected DFT level using the Becke−Perdew86 (BP86) exchange correlation functional.[23] A detailed comparison of different functionals is outside the scope of this study and will be pursued in future work. Unrestricted Kohn−Sham calculations were performed in the case of open-shell doublet systems (i.e., the radical anions). Spin contamination for open-shell systems, monitored by inspection of the expectation value of $\mathbf{S}^2$, was found to be negligible; the maximum discrepancy from the exact value for a doublet, $\langle S^2\rangle = 0.750$, was found to be $\langle S^2\rangle = 0.756$ in the case of {(μ-abpy)[Tc(CO)$_3$Cl]$_2$}$^{\bullet-}$).

All structure optimizations employed the Gaussian98 program.[24] Small-core ECPs and [8s7p6d]/(6s5p3d) valence basis sets were used for Re and Tc,[25] as well as ECPs and DZP valence basis sets for C, N, F, Cl, and Br[26] and a DZV basis for hydrogen.[27]

g-tensors were computed at the optimized structures, using the deMon program[28] and its recently implemented **g**-tensor module.[16] A common gauge origin at the center of mass was employed. Cl, Br, Re, and Tc atoms were described by the same ECPs and valence basis sets[25,26] used in the structure optimizations, combined with all-electron DZVP basis sets for C, N, F, and H (without polarization functions on H).[27] Auxiliary basis sets for the fit of the exchange correlation potential and of charge density[29] were of type (5,2;5,2) for C, N, and F, (5,1;5,1) for H, (3,2;3,2) for Cl and Br, and (3,3;3,3) for Re and Tc. An extra iteration without fit of the exchange correlation potential and with

(16) Malkina, O. L.; Vaara, J.; Schimmelpfennig, B.; Munzarová, M.; Malkin, V. G.; Kaupp, M. *J. Am. Chem. Soc.* **2000**, *122*, 9206.
(17) Malkin, V. G.; Malkina, O. L.; Casida; M. E.; Salahub, D. R. *J. Am. Chem. Soc.* **1994**, *116*, 5898.
(18) Pitzer, R. M.; Winter, N. W. *J. Phys. Chem.* **1988**, *92*, 3061.
(19) Hess, B. A.; Marian, C. M.; Wahlgren, U.; Gropen, O. *Chem. Phys. Lett.* **1996**, *251*, 365.
(20) Schimmelpfennig, B. *Atomic Spin−Orbit Mean-Field Integral Program*; Stockholms Universitet: Stockholm, Sweden, 1996.
(21) Schreckenbach, G.; Ziegler, T. *J. Phys. Chem. A* **1997**, *101*, 3388.
(22) (a) Kaupp, M.; Reviakine, R.; Malkina, O. L.; Arbuznikov, A.; Schimmelpfennig, B.; Malkin, V. G. *J. Comput. Chem.* **2002**, *23*, 794. (b) Neese, F. *J. Chem. Phys.* **2001**, *115*, 11080.
(23) (a) Becke, A. D. *Phys. Rev. A* **1988**, *38*, 3098. (b) Perdew, J. P.; Wang, Y. *Phys. Rev. B* **1986**, *33*, 8822. (c) Perdew, J. P.; Wang, Y. *Phys. Rev. B* **1986**, *34*, 7406.
(24) Frisch, M. J.; Trucks, G. W.; Schlegel, H. B.; Scuseria, G. E.; Robb, M. A.; Cheeseman, J. R.; Zakrzewski, V. G.; Montgomery, J. A., Jr.; Stratmann, R. E.; Burant, J. C.; Dapprich, S.; Millam, J. M.; Daniels, A. D.; Kudin, K. N.; Strain, M. C.; Farkas, O.; Tomasi, J.; Barone, V.; Cossi, M.; Cammi, R.; Mennucci, B.; Pomelli, C.; Adamo, C.; Clifford, S.; Ochterski, J.; Petersson, G. A.; Ayala, P. Y.; Cui, Q.; Morokuma, K.; Malick, D. K.; Rabuck, A. D.; Raghavachari, K.; Foresman, J. B.; Cioslowski, J.; Ortiz, J. V.; Baboul, A. G.; Stefanov, B. B.; Liu, G.; Liashenko, A.; Piskorz, P.; Komaromi, I.; Gomperts, R.; Martin, R. L.; Fox, D. J.; Keith, T.; Al-Laham, M. A.; Peng, C. Y.; Nanayakkara, A.; Gonzalez, C.; Challacombe, M.; Gill, P. M. W.; Johnson, B.; Chen, W.; Wong, M. W.; Andres, J. L.; Gonzalez, C.; Head-Gordon, M.; Replogle; E. S.; Pople, J. A. *Gaussian 98*, Revision A.7; Gaussian, Inc.: Pittsburgh, PA, 1998.
(25) Andrae, D.; Häussermann, U.; Dolg, M.; Stoll, H.; Preuss, H. *Theor. Chim. Acta* **1990**, *77*, 123.
(26) (a) Bergner, A.; Dolg, M.; Küchle, W.; Stoll, H.; Preuss, H. *Mol. Phys.* **1993**, *80*, 1431. (b) d-functions were taken from: *Gaussian Basis Set for Molecular Calculations*; Huzinaga, S., Ed.; Elsevier: New York, 1984.
(27) Godbout, N.; Salahub, D. R.; Andzelm, J.; Wimmer, E. *Can. J. Chem.* **1992**, *70*, 560.
(28) (a) Malkin, V. G.; Malkina, O. L.; Eriksson, L. A.; Salahub, D. R. In *Modern Density Functional Theory: A Tool for Chemistry; Theoretical and Computational Chemistry*; Seminario, J. M., Politzer, P., Eds.; Elsevier: Amsterdam, 1995; Vol. 2. (b) deMon program: Salahub, D. R.; Fournier, R.; Mlynarski, P.; Papai, I.; St-Amant, A.; Ushio, J. In *Density Functional Methods in Chemistry*; Labanowski, J., Andzelm, J., Eds.; Springer: New York, 1991. (c) St-Amant, A.; Salahub, D. R. *Chem. Phys. Lett.* **1990**, *169*, 387.
(29) The notation of the auxiliary basis set is the following: the first value is the number of s primitives and the second is the number of spd shells sharing a common exponent in the case the charge density. The third and fourth values have the same meaning in the case of the exchange correlation potential.

Table 1. Electrochemical and Spectroscopic Data of Complexes $\{(\mu,\eta^2{:}\eta^2\text{-L})[fac\text{-}Re(CO)_3Cl]_2\}^{\bullet-}$

		L = abpy (**1**)	L = abcp (**2**)
$E_{1/2}$(ox) (V)		0.00	+0.09
$E_{1/2}$(red) (V)		−0.80	−0.64
ν_{CO} (cm^{-1})		2017w, 2005s, 1909s, 1885sh	2022w, 2010vs, 1925s,1898s
	(ox):	2044w, 2010vs, 1960sh, 1938m	2028w, 2017vs, 1956br
	(red):		2000s, 1894s, 1863m
λ_{max}/ϵ (nm/10^3 M^{-1} cm^{-1})		631/3.40, 532sh, 497/7.20, 382/13.7	761/3.00, 526/4.45, 468sh, 393/14.9
	(ox):	788/10.99, 710sh, 404/11.1, 332/12.8	903/9.22, 815sh, 420sh, 340/13.5
	(red):		504/2.50, 380/10.8, 312/12.0
g_{iso}		2.0039	2.0054
$a(^{185,187}Re)$ (mT)		2.54	3.3
g_1		2.023	2.039
g_2		2.007	2.001
g_3		1.981	1.976
$\Delta = g_1 - g_3$		0.042	0.063

extended integration grids was performed after SCF convergence in order to obtain accurate Kohn−Sham molecular orbitals at low computational cost.

Whenever computed charges or spin densities are mentioned, we refer respectively to charges derived from natural population analysis[30] and to the Mulliken spin density. Both quantities were computed using Gaussian98 and the same basis set used for the structure optimizations.

Results and Discussion

Preparation of the Radical Complexes and of Neighboring Diamagnetic Species. Both abpy and abcp yielded partially reduced species $\{(\mu\text{-L})[Re(CO)_3Cl]_2\}^{\bullet-}$ when the azo ligands were reacted with $Re(CO)_5Cl$ in chlorinated hydrocarbons. The rather positive reduction potentials of the neutral compounds $\{(\mu\text{-L})[Re(CO)_3Cl]_2\}$ at 0.00 V (abpy complex) and +0.09 V (abcp compound) vs $[Fe(C_5H_5)_2]^{+/0}$ (Table 1) and the reducing capacity of rhenium(I) species are responsible for the radical complex formation at elevated temperatures. Under milder reaction conditions, the diamagnetic compounds $\{(\mu\text{-L})[Re(CO)_3Cl]_2\}$ are obtained exclusively. The new $\{(\mu\text{-abcp})[Re(CO)_3Cl]_2\}$ is assumed to have a structure very similar to that of the crystallographically characterized $\{(\mu\text{-}\eta^2{:}\eta^2\text{-abpy})[fac\text{-}Re(CO)_3Cl]_2\}$, with the chloride ligands in trans (anti) position.[9] Controlled reduction of these neutral compounds with, e.g., cobaltocene or at a cathode produces IR, UV/vis/NIR, and EPR spectroscopic results identical to those of the direct preparations from reaction mixtures.

The complexes $\{(\mu\text{-L})[Re(CO)_3Cl]_2\}$ exhibit intense metal-to-ligand charge-transfer (MLCT) absorptions at very long wavelengths (Table 1). The lower lying π orbital of the abcp ligand in comparison to that of abpy is evident from the bathochromically shifted MLCT band. Reduction to the radical species causes this band to diminish and shift to higher energies (Figure 1, Table 1).

The metal−carbonyl stretching vibrations from IR spectroscopy exhibit the familiar[4,9] low-energy shift on reduction (Table 1).

EPR Spectroscopy. The X-band EPR data of $\{(\mu\text{-abpy})[Re(CO)_3Cl]_2\}^{\bullet-}$ (**1**) were reported earlier.[3,4] The new $\{(\mu\text{-abcp})[Re(CO)_3Cl]_2\}^{\bullet-}$ species (**2**) exhibits a similar 11-line spectrum, however, with a larger isotropic g of 2.0054 (vs 2.0039) and a larger metal hyperfine constant $a(^{185,187}Re) = 3.3$ mT (vs 2.54 mT). Whereas the former effect might be tentatively attributed to the replacement of CH by N or CCl with larger spin−orbit coupling contributions in the bridging radical ligand, the increase in the hyperfine value is probably due to better metal/ligand orbital mixing[5] in the complex with the lower lying singly occupied MO (SOMO). However, this assumption could not be tested in the X-band through determination of the g anisotropy in the glassy frozen state because the overlapping hyperfine lines from the g components produced only an unresolved signal (Figure 2a). We therefore investigated both radical complexes by high-frequency EPR, as illustrated in Figures 2 and 3 and summarized in Table 1.

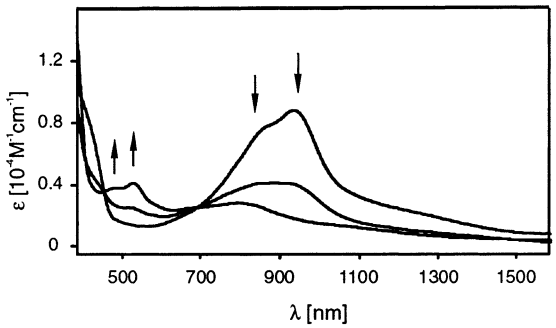

Figure 1. Changes in the absorption spectrum of $(\mu\text{-abcp})[Re(CO)_3Cl]]_2$ on reduction to **2** (OTTLE cell spectroelectrochemistry in CH_2Cl_2/0.1 M Bu_4NPF_6).

Complex **1** exhibits detectable g anisotropy in the W-band (94 GHz), which has been further confirmed by measurements at 230 and 285 GHz (Figure 2b−d). The total amount, $\Delta = g_1 - g_3 = 0.042$, of this anisotropy is distinctly larger than that found for various dicopper(I) complexes of azo-containing radical anions.[31] These results confirm the assumption[4] that the rather unspectacular isotropic g values close to $g_e = 2.002319$ of these organorhenium(I) radicals must be due to a compensation effect. The main contribution causing the relatively large Δ value is the large spin−orbit coupling of the rhenium centers, as will be detailed further in the calculation section. However, there is a clear difference between the abpy radical complex **1** and the abcp analogue **2**, which was also studied at 285 GHz (Figure 3). Complex **2**, with the better π-accepting bridging ligand, displays a still larger anisotropy, $\Delta = 0.063$, thus supporting the interpretation given above in terms of enhanced metal/ligand orbital mixing. As with the abpy analogue, a rhombic pattern with both negative and posive **g**-shift components is observed, which was similarly found for dicopper(I)

(30) Reed, A. E.; Weinhold, F. *J. Chem. Phys.* **1985**, *83*, 1736. Reed, A. E.; Curtiss, L. A.; Weinhold, F. *Chem. Rev.* **1988**, *88*, 899.

(31) Barra, A.-L.; Brunel, C.; Baumann, F.; Schwach, M.; Moscherosch, M.; Kaim, W. *J. Chem. Soc., Dalton Trans.* **1999**, 3855.

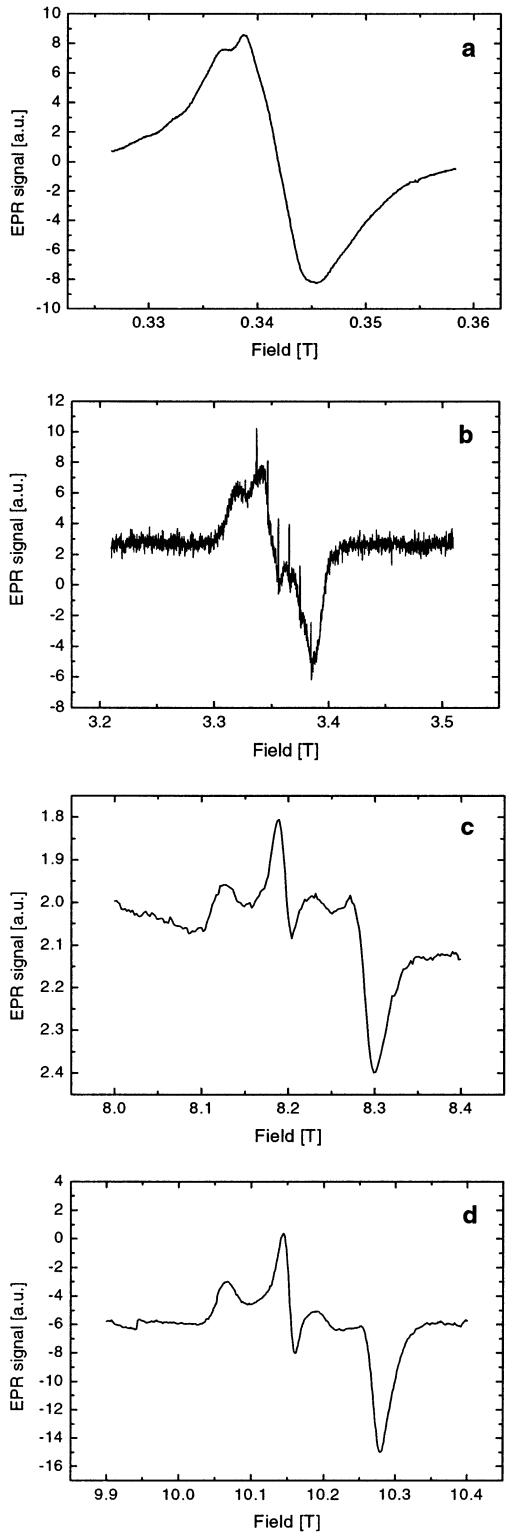

Figure 2. EPR spectrum of **1** at 9.5 GHz in CH_2Cl_2 (a), at 94 GHz in toluene (b), and at 230 (c) and 285 GHz (d), both in CH_2Cl_2/toluene (1/1).

complexes of azo-containing radicals but not for tetrazine-bridged species.[31]

Computed Structures, Energies, and Spin Distributions. The essential geometrical parameters from DFT-optimized structures of the free ligands and of the complexes in their neutral and radical anion forms are reported in Table 2. For the labeling scheme see formulas 1 and 2.

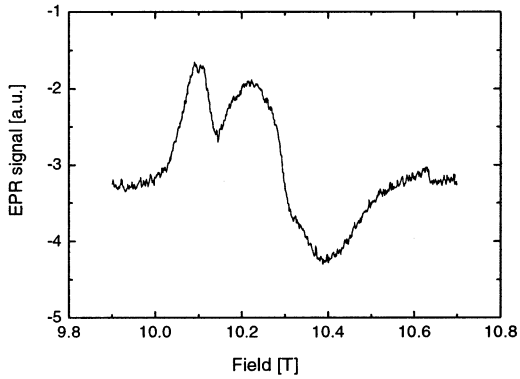

Figure 3. EPR spectrum of **2** at 285 GHz in CH_2Cl_2/toluene (1/1).

Direct comparison with X-ray data is possible for the neutral free ligands[32] and for *trans*-(μ-abpy)[$Re(CO)_3Cl]_2$.[9] In all three cases, good agreement between experimental and calculated values is found (the largest deviations in the bond lengths do not exceed 0.04 Å), as expected at this level of theory. In particular, the arrangement at the metal-to-ligand interface and the typical steric effects which lead to a slight twist of the abpy ligand in order to avoid C^3—H···CO_{eq} interactions[33] are correctly reproduced.

When comparing the optimized structures of (μ-abpy)[$Re(CO)_3Cl]_2$ and of (μ-abcp)[$Re(CO)_3Cl]_2$, it is remarkable that the twisting of the ligand is strongly reduced in the latter where the sterically active C^3-H group has been replaced by N; the torsional angle $N^1-C^2-N_{azo}-N_{azo}$ is 8.7° for the abpy complex (experimental value 9.4°) but 3.6° for the abcp analogue. The other structural parameters and the coordination sphere around rhenium are rather similar. A slight shortening of the $Re-N_{azo}$ bond by 0.019 Å and an even slighter lengthening on the $N_{azo}-N_{azo}$ bond by 0.006 Å can be noted for the abcp complex.

In contrast, a comparison of the calculated structures of the neutral free ligands with those in the complexes shows, in the cases of both abpy and abcp, a significant elongation of the $N_{azo}-N_{azo}$ bond (0.06 Å for the abpy compound and 0.07 Å for the abcp system). This effect has already been underscored experimentally both for (μ-abpy)[$Re(CO)_3Cl]_2$ [9] and for a dinuclear Cu^I complex of abpy.[33] The lengthening was ascribed to significant π back-bonding from the metal d_π orbitals to the π^* MO of the ligand. To better illustrate this point, a qualitative representation of the relevant MOs with only the metal-to-azo ligand π interactions is shown in Figure 4.

The linear combinations of the two metal d orbitals having the correct symmetry to interact with the π and π^* MOs of the ligand are labeled as d and d* to underline the d−d metal−metal interaction type (bonding or antibonding, respectively). The (d−π) MO corresponds to the π metal−ligand bonding orbital, while the (d*−π^*) MO is what is commonly defined as a π^* back-bonding orbital. In fact, due to the mixing of metal and ligand AOs in this orbital, a significant amount of electron density is transferred from the metal to the ligand. When the π^* empty orbital of the ligand gets lower in energy, the (d*−π^*) MO starts to have a larger ligand contribution. Consequently, a larger amount of charge is transferred. As the π^*

(32) (a) Bock, H.; Dienelt, R.; Schödel, H.; Van, T. T. H. *Struct. Chem.* **1998**, *9*, 279. (b) Doslik, N.; Sixt, T.; Kaim, W., unpublished.
(33) Kaim, W.; Kohlmann, S.; Jordanov, J.; Fenske, D. *Z. Anorg. Allg. Chem.* **1991**, *598/599*, 217.

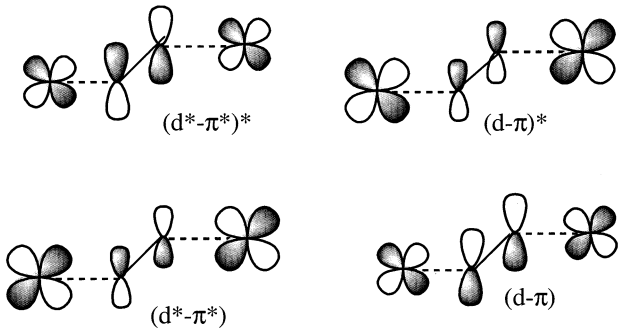

Figure 4. Qualitative MO interaction diagram showing the metal-to-ligand π bonding and back-bonding interactions.

orbital is a $N_{azo}-N_{azo}$ antibonding orbital, a lengthening of this bond is expected. This effect is calculated to be larger in the case of abcp complexes, indicating better metal−ligand π back-bonding interaction relative to that in abpy analogues.

An estimate of the binding properties of the two neutral ligands can be derived from their molecular orbital diagram (Figure 5). When going from abpy to abcp, a stabilization of both the π orbital (by 542 meV) and the π^* level (by 571 meV) is observed. These orbitals are those involved in the $\pi-$d donating and d$-\pi^*$ back-donating interactions in the complexes (see Figure 4). The corresponding σ donor orbitals (N lone pairs) are also substantially lowered in energy by 218 meV for the abcp system.

On the basis of these orbital shifts, a stronger interaction and a larger transfer of electron density from the metal to the ligand are expected with the abcp bridge. Consequently, the computed charge on the Re atoms increases from −0.177 for (μ-abcp)-$[Re(CO)_3Cl]_2$ to −0.158 for (μ-abpy)$[Re(CO)_3Cl]_2$.

A more quantitative measure of the capability of a ligand to "soak up" electrons has been given recently by Parr et al.[34] These authors, following a qualitative suggestion of Maynard,[35] have proposed an electrophilicity index, ω, which measures the response of a ligand toward the partial transfer of electron density, i.e., what happens in the case of back-bonding.

Following Parr, the electrophilicity index is defined, within the ground-state parabola model, as

$$\omega \equiv \frac{\mu^2}{2\eta} \approx \omega_{GS} = \frac{(I+A)^2}{8(I-A)} \qquad (5)$$

where μ is the chemical potential, η the chemical hardness, A the electron affinity, and I the ionization potential. A and I have been evaluated within the adiabatic approximation; i.e., the ligand cation (L^+) and anion (L^-) energies were computed at the neutral ligand geometry. The computed values of ω for abpy and abcp are 1.52 and 1.96 eV, respectively, thus confirming the better acceptor character of abcp. Although not equivalent, the electrophilicity index is related to the capability of the neutral species to accept one electron, i.e., to its electron affinity. As expected, the abcp compounds have higher electron affinities than the corresponding abpy complexes (1.83 eV for abcp relative to 1.17 eV for abpy, and 3.65 eV for (μ-abcp)[Re-$(CO)_3Cl]_2$ relative to 3.32 eV for (μ-abpy)$[Re(CO)_3Cl]_2$).

Furthermore, the complexes are computed to be more easily reduced than the corresponding free ligands, in agreement with the experimental reduction potentials. While structural relaxation and solvation[36] are not taken into account in this model (adiabatic approximation), the data clearly suggest that the abcp compounds will be reduced more easily. Effects of nonadiabatic reduction can be included by considering the energy differences (including zero-point energy correction) between optimized neutral and reduced species. In this case, $abpy^{\bullet-}$ is found to be 1.24 eV more stable than abpy, and $abcp^{\bullet-}$ 2.23 eV more stable than abcp.

In the free ligands, the $N_{azo}-N_{azo}$ and $N_{azo}-C^2$ bond lengths are affected most by reduction. In particular, an elongation of the $N_{azo}-N_{azo}$ distance by 0.062 Å in both instances and an increase of the $N_{azo}-C^2$ distance by 0.054 and 0.060 Å are found for $abpy^{0/\bullet-}$ and $abcp^{0/\bullet-}$, respectively. These changes are consistent with a population of the π^* orbital upon reduction.

In the free ligand radical anions, the spin density is mainly located on the nitrogen atoms, both at the azo group (dominant contribution, 0.2 on each nitrogen) and in the pyridine (0.1 on nitrogen) or pyrimidine (0.1 on each nitrogen) ring. However, a non-negligible contribution arises from C^3 (0.06) and C^5 (0.15) in $abpy^{\bullet-}$ and from C^5 (0.15) and Cl (0.01) in $abcp^{\bullet-}$. In particular, the spin density found on the N^1 and Cl atoms of $abcp^{\bullet-}$ is similar to that found on the corresponding C^3H group and H atom of abpy $^{\bullet-}$. Therefore, and due to the larger spin−orbit coupling of Cl and N atoms compared to C, we may expect a larger **g**-shift already in the case of free $abcp^{\bullet-}$ compared to $abpy^{\bullet-}$ (see below).

The complexes show a similar behavior upon reduction, confirming that the extra electron populates mainly the (d−π^*)* ligand-centered MO (see Figure 4). In particular, the $N_{azo}-N_{azo}$ bond is elongated ($\Delta(N_{azo}-N_{azo}) = 0.030$ Å for (μ-abpy)$[Re(CO)_3Cl]_2$ and 0.025 Å for (μ-abcp)$[Re(CO)_3Cl]_2$), similar to the results for the free ligands (see above). On the other hand, the metal coordination sphere (i.e., the rhenium−chlorine or rhenium−carbonyl bond lengths) is only slightly affected by reduction. Furthermore, the comparison within the extended series $\{(\mu\text{-abcp})[Re(CO)_3Cl]_2\}^{\bullet-}$ (X = F, Cl, Br) shows that the halogen atom variation has practically no structural effect and does not change the coordination sphere at rhenium (except, of course, for the different M−X bond lengths).

Confirmation for a predominantly but not exclusively ligand-centered reduction is also provided by the analysis of the Mulliken spin densities computed for the different complex radical anions (Table 3). Ligand contributions to the spin density range from 67% in $\{(\mu\text{-abcp})[Re(CO)_3Cl]_2\}^{\bullet-}$ to 86% in (μ-abpy)$[Tc(CO)_3Cl]_2\}^{\bullet-}$. These results already indicate non-negligible spin delocalization onto the metal fragment. Most notably, the delocalization is more pronounced for abcp systems compared to abpy analogues. For example, only ca. 73% of the spin density remains on the abcp ligand in **2**, as compared to ca. 83% on the abpy ligand in **1**.

While the halogen substituents have essentially no structural effect, their different electronegativities are reflected by the different amount of spin density delocalized onto them and onto the metals. The computed spin density for the radical complexes

(34) Parr, R. G.; Szentpály, L. v.; Liu, S. *J. Am. Chem. Soc.* **1999**, *121*, 1922.
(35) Maynard, A. T.; Huang, M.; Rice, W. G.; Covel, D. G. *Proc. Natl. Acad. Sci. U.S.A.* **1998**, *95*, 11578.
(36) Winget, P.; Weber, E. J.; Cramer, C. J.; Truhlar, D. G. *Phys. Chem. Chem. Phys.* **2000**, *2*, 1231.

Table 2. Main Structural Parameters of Optimized Ligands (L) and Complexes $\{(\mu\text{-L})[Re(CO)_3X]_2\}$ in the Neutral and Radical Anion Forms[a]

	abpy	abpy$^{\bullet-}$		abcp	abcp$^{\bullet-}$
$N_{azo}-N'_{azo}$	1.269 (1.246)	1.331	$N_{azo}-N'_{azo}$	1.268 (1.230)	1.331
C^2-N_{azo}	1.425 (1.432)	1.371	C^2-N_{azo}	1.426 (1.439)	1.366
C^2-N^1	1.345 (1.335)	1.377	C^2-N^1	1.347 (1.331)	1.379
C^2-C^3	1.413 (1.394)	1.435	C^2-N^3	1.347(1.331)	1.379
C^3-C^4	1.395 (1.377)	1.389	C^4-N^3	1.336 (1.335)	1.325
C^4-C^5	1.405 (1.385)	1.415	C^4-C^5	1.403 (1.391)	1.408
C^5-C^6	1.405 (1.386)	1.408	C^5-Cl	1.756 (1.721)	1.789
C^6-N^1	1.339 (1.332)	1.334	C^5-C^6	1.403 (1.387)	1.408
$\alpha(N_{azo}-N_{azo}-C^2)$	113.6 (114.1)	114.4	C^6-N^1	1.336 (1.325)	1.325
			$\alpha(N_{azo}-N'_{azo}-C^2)$	113.2 (113.89)	113.6

	$\{(\mu\text{-abpy})[Re(CO)_3Cl]_2\}$	$\{(\mu\text{-abpy})[Re(CO)_3Cl]_2\}^{\bullet-}$	$\{(\mu\text{-abcp})[Re(CO)_3Cl]_2\}$	$\{(\mu\text{-abcp})[Re(CO)_3Cl]_2\}^{\bullet-}$
M−X	2.493 (2.459)	2.527	2.483	2.521
$M-CO_{eq}$[b]	1.952 (1.933)	1.928	1.952	1.931
$M-CO_{ax}$	1.948 (1.937)	1.931	1.953	1.934
$M-N_{azo}$	2.177 (2.134)	2.231	2.158	2.203
M−N	2.166 (2.135)	2.177	2.163	2.179
M−M	5.123 (5.003)	5.228	5.115	5.196
$N_{azo}-N'_{azo}$	1.329 (1.304)	1.359	1.335	1.356

	$\{(\mu\text{-abcp})[Re(CO)_3F]_2\}^{\bullet-}$	$\{(\mu\text{-abcp})[Re(CO)_3Br]_2\}^{\bullet-}$	$\{(\mu\text{-abpy})[Tc(CO)_3Cl]_2\}^{\bullet-}$	$\{(\mu\text{-abcp})[Tc(CO)_3Cl]_2\}^{\bullet-}$
M−X	2.041	2.671	2.516	2.512
$M-CO_{eq}$[b]	1.928	1.931	1.921	1.909
$M-CO_{ax}$	1.947	1.931	1.921	1.914
$M-N_{azo}$	2.201	2.201	2.230	2.199
M−N	2.177	2.177	2.170	2.173
M−M	5.192	5.195	5.215	5.170
$N_{azo}-N'_{azo}$	1.358	1.357	1.352	1.349

[a] Available X-ray data (from refs 31 and 9) are reported in parentheses. Bond lengths in angstroms, angles in degrees. [b] Average distance.

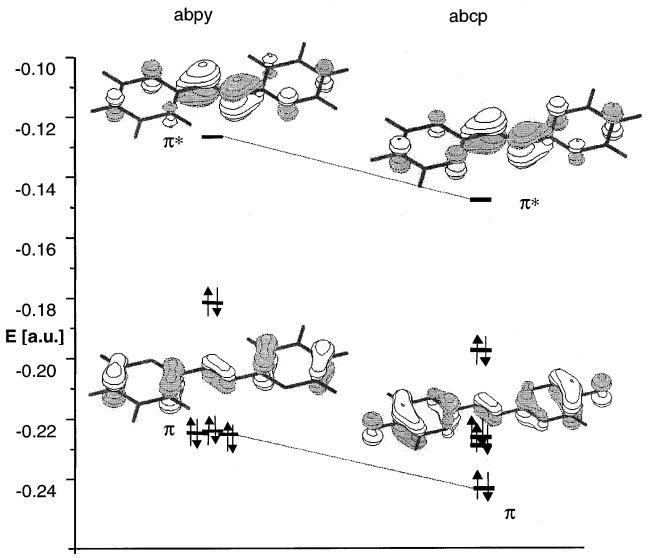

Figure 5. Molecular orbital energy diagram for abpy and abcp (molecular orbital isosurface contour value ± 0.05 $(e/Å^3)^{1/2}$).

$\{(\mu\text{-abcp})[Re(CO)_3X]_2\}^{\bullet-}$ shows a continuous decrease on the metals (from ∼18% to ∼13%) but an increase on X (from ∼3.5% to ∼6.5%) when going from X = F to X = Br.

g-Tensor Results. In Table 4, the calculated **g**-tensors are compared to the experimental data (numbers in parentheses), both for the free ligands and for the complexes. An understanding of the general trends of the **g**-tensor results is aided by the spin density analyses (Table 3) and, in addition, by the breakdown of $\Delta\mathbf{g}_{SO/OZ}$ in terms of atomic contributions (see Table S1, Supporting Information).

As is generally accepted,[16] the main contribution to the **g**-shifts comes from the $\Delta\mathbf{g}_{SO/OZ}$ term, which is between 1 and 2 orders of magnitude larger than both the gauge ($\Delta\mathbf{g}_{GC}$) and the relativistic mass ($\Delta\mathbf{g}_{RMC}$) corrections. Therefore, we will focus mainly on the atomic contributions to $\Delta\mathbf{g}_{SO/OZ}$ in the analysis of the **g**-shifts. For the free ligands, the computed g_{iso} values lie in the same region as the measured data within experimental error (± 0.0005).[3,4,32b] Larger deviations (up 0.02 in **g**-shift in the case of **2**) pertain to the two experimentally observed organorhenium complexes. In agreement with experiment, the isotropic g value increases from abpy- to abcp-containing systems, and from free ligand radicals to the paramagnetic complexes.

A small anisotropy is computed for the free ligands ($\Delta = g_1 - g_3 = 0.0041$ and 0.0060 for abpy and abcp, respectively), consistent with expectation for organic π radicals with the largest SO coupling contribution coming from nitrogen. The corresponding $Re(CO)_3Cl$ complexes are calculated to have an anisotropy roughly 1 order of magnitude larger (0.035 and 0.042 for the abpy and abcp complexes **1** and **2**, respectively). Among the free ligand radicals, the larger g anisotropy computed for abcp$^{\bullet-}$ is mainly related to the presence of the two chlorine atoms, which give a substantial contribution to $\Delta\mathbf{g}_{SO/OZ}$ (cf. Table S1), despite very little spin density.

For the complexes, the calculations apparently underestimate the g anisotropy (0.035 vs 0.042 (expt) for **1**, and 0.054 vs 0.063 (expt) for **2**) while overestimating g_{iso} (2.0121 vs 2.0039 (expt) for **1**, 2.0262 vs 2.0054 (expt) for **2**). Individual comparison of the computed components with the HF-EPR results highlights that the calculations typically overestimate the largest component less than the two smaller ones (the sign of Δg_2 for **2** is not correctly reproduced), resulting in the underestimated g anisotropy. Most importantly, the increase in anisotropy from **1** to **2** is reproduced with good accuracy (see below). Substitution of Re by Tc provides smaller g_{iso} values and reduced anisotropy. This is due both to smaller spin−orbit coupling of Tc relative

Table 3. Computed Mulliken Spin Densities in Complexes $\{(\mu\text{-L})[Re(CO)_3X]_2\}^{\bullet-}$ [a]

	$\{(\mu\text{-abpy})[Re(CO)_3Cl]_2\}^{\bullet-}$	$\{(\mu\text{-abcp})[Re(CO)_3F]_2\}^{\bullet-}$	$\{(\mu\text{-abcp})[Re(CO)_3Cl]_2\}^{\bullet-}$	$\{(\mu\text{-abcp})[Re(CO)_3Br]_2\}^{\bullet-}$
L	0.8342	0.6657	0.7264	0.7227
2×Re	0.0589	0.1783	0.1363	0.1304
2×X	0.0350	0.0350	0.0482	0.0633
6×CO	0.0720	0.1210	0.0890	0.0836

	$\{(\mu\text{-abpy})[Tc(CO)_3Cl]_2\}^{\bullet-}$	$\{(\mu\text{-abcp})[Tc(CO)_3Cl]_2\}^{\bullet-}$
L	0.8693	0.7459
2×Tc	0.0471	0.1491
2×X	0.0336	0.0305
6×CO	0.0500	0.0745

[a] 2×Re (Tc), 2×X, 6×CO, L denote contributions from the two metal atoms, the two halogen (X) ligands, the six CO ligands, and the bridging ligands (L = abpy, abcp), respectively.

Table 4. Computed **g**-Tensors (in Principal Axes) for $L^{\bullet-}$ and $\{(\mu\text{-L})[M(CO)_3X]_2\}^{\bullet-}$ (Experimental Values in Parentheses)

	g_{iso}	g_1	g_2	g_3	$\Delta = g_1 - g_3$
$abpy^{\bullet-}$	2.0039 (2.0044)	2.0064	2.0030	2.0023	0.0041
$abcp^{\bullet-}$	2.0045 (2.0041)	2.0080	2.0037	2.0020	0.0060
$\{(\mu\text{-abpy})[Re(CO)_3Cl]_2\}^{\bullet-}$ (**1**)	2.0121 (2.0039)	2.0291 (2.023)	2.0128 (2.007)	1.9945 (1.981)	0.035 (0.042)
$\{(\mu\text{-abcp})[Re(CO)_3Cl]_2\}^{\bullet-}$ (**2**)	2.0262 (2.0054)	2.0536 (2.039)	2.0250 (2.001)	2.0001 (1.976)	0.054 (0.063)
$\{(\mu\text{-abcp})[Re(CO)_3F]_2\}^{\bullet-}$	2.0395	2.0655	2.0586	1.9944	0.071
$\{(\mu\text{-abcp})[Re(CO)_3Br]_2\}^{\bullet-}$	2.0356	2.0736	2.0257	2.0076	0.066
$\{(\mu\text{-abpy})[Tc(CO)_3Cl]_2\}^{\bullet-}$	2.0052	2.0114	2.0044	1.9998	0.012
$\{(\mu\text{-abcp})[Tc(CO)_3Cl]_2\}^{\bullet-}$	2.0093	2.0193	2.0047	2.0039	0.015

to Re and to a reduced spin density on the metal (less covalent interaction; cf. Table 3). On the other hand, both g_{iso} and the anisotropy increase upon going from F to Br in $\{(\mu\text{-abpy})[Re(CO)_3X]_2\}^{\bullet-}$.

As already underlined by the structural features, the spin density in the complex radical anions is mainly localized on the ligands (Table 3) but non-negligibly delocalized onto the metal and onto the metal-bound halogen substituents X (by up to 21%). The delocalization is larger for abcp than for abpy complexes, and larger for Re than for Tc compounds. Due to the dominant spin−orbit coupling contribution from the metals (and partially from the heavier halogen atoms), even a moderate spin density on the fragments $M(CO)_3X$ will cause considerable **g**-shifts. Contributions from M and X are thus responsible for the differences in computed **g**-tensors along the $\{(\mu\text{-abcp})[Re(CO)_3X]_2\}^{\bullet-}$ series. Indeed, the atomic analysis of the $\Delta\mathbf{g}_{SO/OZ}$ contributions for **1** and **2** (cf. Table S1) indicates that the largest contributions are due to the Re and Cl atoms (at least 1 order of magnitude larger than the other contributions), although more than 70% of the spin density is localized on the bridging azo ligand. The *g* anisotropy is also dominated by metal and chlorine contributions.

Figure 6 shows the sum of the computed spin density vs the **g**-tensor anisotropy for different halogen substituents X in the $\{(\mu\text{-abcp})[Re(CO)_3X]_2\}^{\bullet-}$ series. An essentially parallel trend in these two quantities is observed. Counterintuitively, the *g* anisotropy does not change monotonically from F via Cl to Br complexes: While the spin density on X increases linearly, the metal spin density changes substantially from F to Cl but only very slightly from Cl to Br. The chlorine compound has the smallest *g* anisotropy and the largest spin density on the bridging ligand, whereas the fluorine complex is predicted to have the largest *g* anisotropy and metal spin density.

Further important information available from the calculations pertains to the orientation of the principal axes of the **g**-tensor relative to the molecular framework. For the free ligand radical anions, the **g**-tensor is oriented with the smallest component

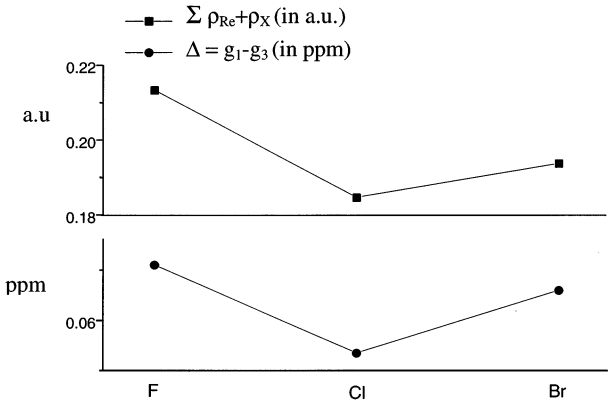

Figure 6. Plot of the sum of the computed Mulliken spin densities on Re and X (X = F, Cl, Br) atoms vs the **g**-tensor anisotropy as a function of X for $\{(\mu\text{-abcp})[Re(CO)_3X]_2\}^{\bullet-}$.

(g_3) perpendicular to the ligand plane and the other two components in-plane (the g_2 component is almost parallel to the C^2N bond). This orientation is in agreement with qualitative rules[11] for π radicals.

The $abpy^{\bullet-}$ complexes of $M(CO)_3Cl$ (M = Re, Tc) exhibit essentially unaltered orientation. However, the computed **g**-tensor orientation of the abcp complexes differs substantially! While the largest component (g_1) lies still in the ligand plane, g_2 does not. As a consequence, the smallest component (g_3) is no longer perpendicular to the ligand plane. This effect is remarkably pronounced in the case of $\{(\mu\text{-abcp})Re(CO)_3F]_2\}^{\bullet-}$, where g_3 exhibits an angle of 54° with the ligand plane. The angle increases to 74° and 84° in the case of **2** and $\{(\mu\text{-abpy})[Re(CO)_3Br]_2\}^{\bullet-}$, respectively. This change in orientation is entirely due to the metal and halogen contributions, as shown by the atomic analyses. For this reason, we have reported the atomic contributions in the general, not in the principal axes system. The orientations of the individual contributions from L and the metal fragments differ, and thus the components would not add up correctly in the principal axes system.

Summarizing, the calculations show clearly that the increased *g* anisotropy in the complexes as compared to that in the free ligand radical anions derives predominantly from the spin−orbit coupling effects of the metal atoms, with some contributions also from the metal-bound halogen ligands. Moreover, the increased *g* anisotropy of abcp compared to abpy complexes is clearly due to an enhanced metal contribution because of larger spin density on the $M(CO)_3X$ fragments. The enhanced contribution from these fragments is also responsible for the altered orientation of the **g**-tensor in the abcp complexes. Clearly, the higher *g* anisotropy in **1** (expt, $\Delta = 0.042$; calcd, 0.035) as compared to that of $\{(\mu\text{-abpy})[Cu(Ph_2P(CH_2)_6PPh_2)]_2\}^{\bullet+}$, with $\Delta = 0.0166$,[31] is related to the larger spin−orbit coupling constant of Re^{I} in comparison to that of Cu^{I}.[6] As a chemically immediately relevant result of this study, the long assumed[3] but experimentally difficult to quantify spin transmission from the radical ligands via rhenium to the halide ligands could now be established, bearing direct implications on the reductive activation mechanism in these potential catalytic intermediates.[1−5]

Future theoretical work will deal (a) with the validation of different density functionals (we have preliminary indications that hybrid functionals[22] may provide improved quantitative accuracy for the **g**-tensors) and (b) with improved analyses in terms of individual MO contributions or excitations within the sum-over-states expression for $\Delta\mathbf{g}_{SO/OZ}$ (e.g., the question of positive and negative **g**-shift components). We are furthermore currently carrying out extended studies of other related mono- or dinuclear complexes with predominantly ligand-centered spin density. In general, the combination of high-frequency EPR studies with DFT calculations is envisaged as a very promising approach for the analysis of radical complexes containing heavy elements.

Acknowledgment. This work was supported by the Deutsche Forschungsgemeinschaft (DFG) within the Priority Program "High-Field EPR" (Ka 618/19 and Ka 1187/4) and the Graduate College "Magnetische Resonanz". Support from the Fonds der Chemischen Industrie and from the European Community "Access to Research Infrastructure Action of the Improving Human Potential Programme" is also gratefully acknowledged.

Supporting Information Available: Table S1, showing the breakdown of the $\Delta\mathbf{g}_{SO/OZ}$ contributions to the **g**-shifts in terms of fragment contributions (PDF). This material is available free of charge via the Internet at http://pubs.acs.org.

JA025829N